

**Supplementary Material for:**

**Comprehensive quantitative analysis of erythrocytes and leukocytes using trace volume of human blood using microfluidic-image cytometry and machine learning**

Nima Moradi<sup>1#</sup>, Fateme Haji Mohamad Hoseyni<sup>1#</sup>, Hassan Hajghassem<sup>1\*</sup>, Navid Yarahmadi<sup>1</sup>, Hadi Niknam Shirvan<sup>1</sup>, Erfan Safaie<sup>1</sup>, Mahsa Kalantar<sup>1</sup>, Salma Sefidbakht<sup>2</sup>, Ali Amini<sup>3</sup>, Sebastiaan Eeltink<sup>3</sup>

<sup>1</sup>University of Tehran, Faculty of New Sciences and Technologies, Tehran, Iran

<sup>2</sup>University of Tehran, Department of Pathology, Tehran, Iran

<sup>3</sup>Vrije Universiteit Brussel, Department of Chemical Engineering, Brussels, Belgium

(#) shared first authorship

(\*) Corresponding author: E-mail: [hajghassem@ut.ac.ir](mailto:hajghassem@ut.ac.ir); University of Tehran, Faculty of New Sciences and Technologies, North Kargar Street, Tehran, Iran

## 1. Image processing and CNN classification

### 1.1. Image processing and cell detection

To identify the optimal method for detecting cells in the images (Fig. S1A), first the images the image was converted to binary format. As a result, the noise of the images was reduced. The Otsu method was applied to analyze each image individually, calculate the threshold, and generating the binary mask, see Fig. S1B). The contours in the mask were separated with the desired features and by combining the mask with the original image according to the bitwise-AND operation, the cells were identified and placed in frames with dimensions of  $256 \times 256$  pixels, see Fig. S1C).

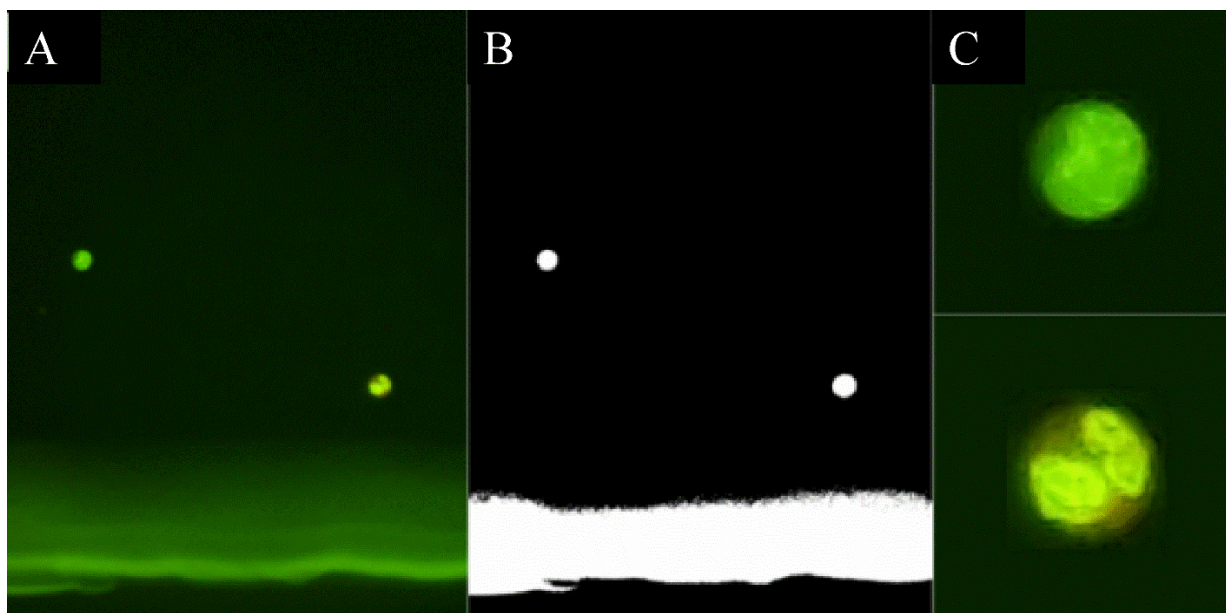


**Figure S1.** Image processing of raw data and cell detection, A) Raw figure of two WBCs, B) Binary mask after applying the Otsu method, C) Output of bitwise-AND operation between mask and original image, and locate single cells in a frame.

### 1.2. CNN design and optimizing training model

The CNN design structure features 4 convolution layers and 2 fully-connected layers, as shown in Fig. S2. Pooling operation is performed after the first layer of convolution, visualized by the red planes. Note, the first layer has not been pooled which significantly increase accuracy. After each layer of convolution, the max-pooling operation was performed to reduce the image size. The input size is (32, 32, 3) and the generated output by the convolutional network is (4, 4,

256). Consequently, the number of features categorized at the input of the fully-connected layer are  $4 \times 4 \times 256 = 4096$ . To consider more details by the network the dimensions of the convolution kernels have been set  $3 \times 3$ . To reach the highest accuracy the number of layers and running time were systematically varied, resulting in the optimized CNN represented in Fig. S2.

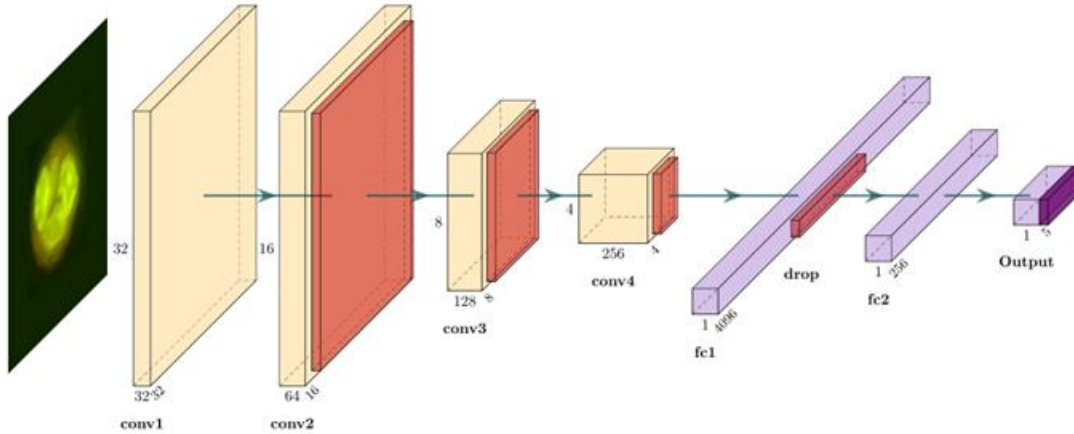


**Figure S2.** Neural network design with four convolution layers and two fully-connected layers.

The original of WBCs subtypes' images was 1078. Increasing the number of images, by rotating and flipping photos, has a tremendous effect on the accuracy of the network, as the accuracy of the network increased about 8% from 90.27% to 98.57%. Fig. S3 shows the training profile where the model accuracy is depicted as function of epochs by using 5093 images as training set and 1260 images as test set. Adam's optimization algorithm was applied and a learning rate of 0.00001 was selected in the initial stage, which led to fast convergence in the early stages. The high training rate causes overfitting error, see the orange graph fluctuation in epoch 25 to 75. With the exponential reduction of the learning rate in the next stages, the accuracy of testing set converges with the training set, and overfitting was reduced in epoch 75 to 150. To ensure robust training, the batch size of every 5 steps was doubled and finally fixed. The loss function of the categorical cross-entropy model was used.

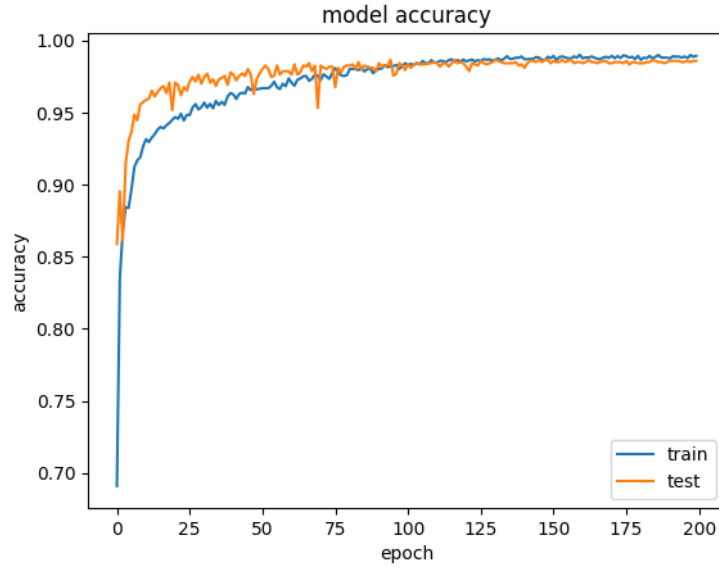


**Figure S3.** Robustness of the CNN model showing the accuracy of the training and test data as function of epoch.

### 1.3. CNN model evaluation

Table S1 below shows the accuracy and precision of CNN-model for detection of WBCs. The diagonal section shows the correct prediction and rest of the table refer to wrong predictions.

**Table S1.** Confusion matrix for neutrophil (Neu), lymphocyte (Lym), monocyte (Mon), eosinophil (Eos), and basophil (Bas).

Test Input	Bas	4	0	0	0	0
	Eos	0	25	0	0	1
	Lym	0	0	487	4	0
	Mon	0	0	2	142	1
	Neu	0	3	0	1	590
		Bas	Eos	Lym	Mon	Neu
		Model prediction				

The model performance is calculated based on the results from above figure. Accuracy, recall, precision, and specificity are calculated based on these formulas:

$$\text{Eq. 1: Accuracy} = \frac{TP+TN}{TP+TN+FP+FN}$$

$$\text{Eq. 2: Recall} = \frac{TP}{TP+FN}$$

$$\text{Eq. 3: Precision} = \frac{TP}{TP+FP}$$

$$\text{Eq. 4: specificity} = \frac{TN}{TN+FP}$$

Where “TP” (true positives) refers to samples that model could correctly predict the positive class, “TN” (true negatives) refers to samples that correctly predict the negative class, “FP” (false positives) is an outcome where the model incorrectly predicts the positive class, and “FN” (false negative) indicates when the model incorrectly predicts the negative class. Accuracy is a criterion that generally describes how the model works in all classes. Recall examines how a class is classified. Precision specifies a criterion to evaluate the accuracy of network performance in each class. Specificity also examines the performance of the network in predicting another class. These parameters are obtained according to the definition from the confusion matrix data of Table S2. Table S2 indicates that the model is highly accurate for classifying basophiles and lymphocytes. The recall for monocytes and eosinophiles is slightly lower than for other WBC subpopulations, due to the lower number of training images used. The lower recall value neutrophiles is because of its similarity structure to monocytes and eosinophiles.

**Table S2.** Model performance of each subpopulation of WBC’s.

Groups	Accuracy (%)	Recall (%)	Precision (%)	Specificity (%)
Neutrophil	99.32	99.49	99.15	99.24
Lymphocyte	99.19	100.00	98.37	99.78
Monocyte	97.99	93.46	98.62	99.81
Eosinophil	96.15	88.88	92.30	99.83
Basophil	100.00	100.00	100.00	100.00

## 2. RBC and WBC counting

### 2.1. cell sedimentation and monolayer formation

The sedimentation of cells in the microchannel forming a monolayer took less than 2 min. Figure S4A-B shows macroscopic image of cells right after and 2 min after injection of the sample, respectively.

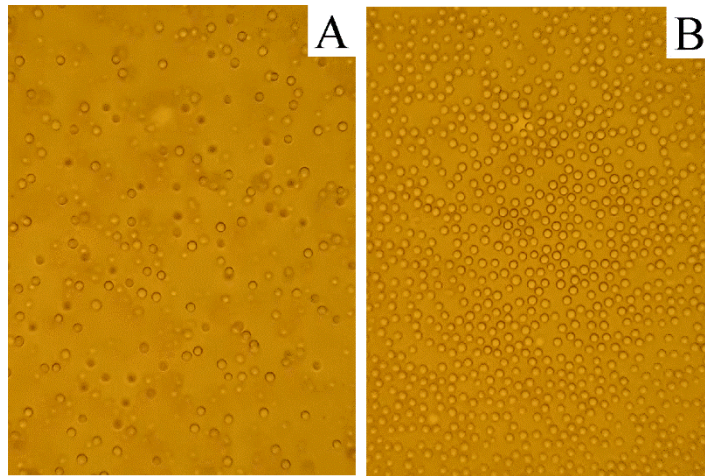


**Figure S4.** Photographs of the formation of a monolayer of blood cells (A) during sedimentation and (B) after 2 min of settling.

Results for determining the minimum number of microscopy images to yield accurate RBC's and WBC's count while minimizing the processing time was shown in Figure 5A-B, respectively.

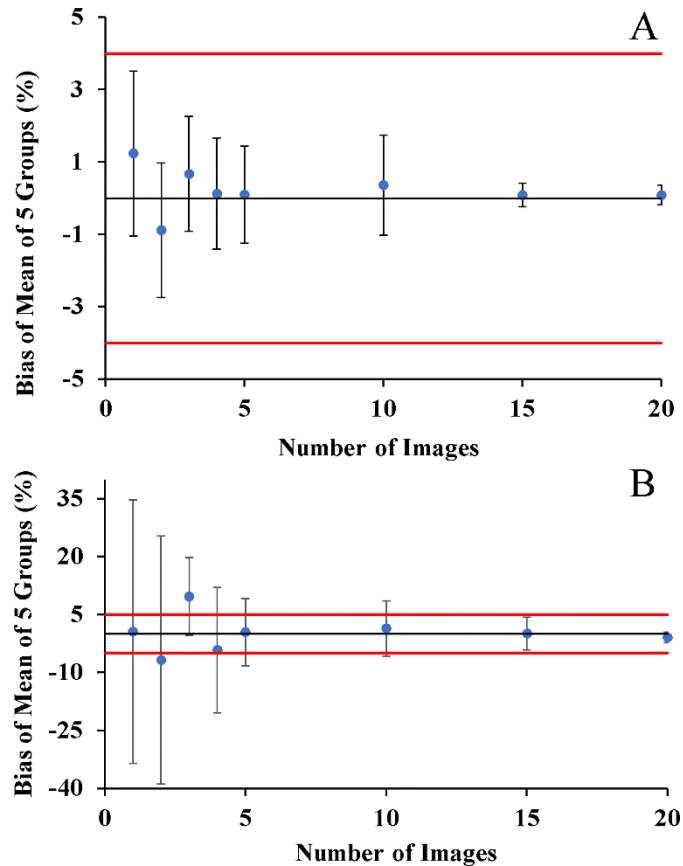


**Figure S5.** Bias analysis for total count number of (A) RBC's and (B) WBC's present in whole blood after sphering and fixation as a function of the number of microscopic images analyzed. Each microscopy image contains on average 2000 RBC's and 40 WBC's. The error bar on the data points represents the 95% confidence interval for  $n = 5$ . The striped lines represent the 4% in (a) and 5% in (b) intervals defined as acceptable variation in hematology readout defined by CLIA.

### 3. Validation of experimental result with clinical results

The corresponding correlation analysis plots for the RBC count MCV, HCT, RDW-CV, and RDW-SD is depicted in the Fig. S6, and for WBC's including subpopulations in Fig. S7. The solid red lines show the 95% confidence interval and dotted blue line shows the bias. Most data points fall within the error margin of the hematology analyzer. The error bars visualize the measurement repeatability ( $n = 5$ ).

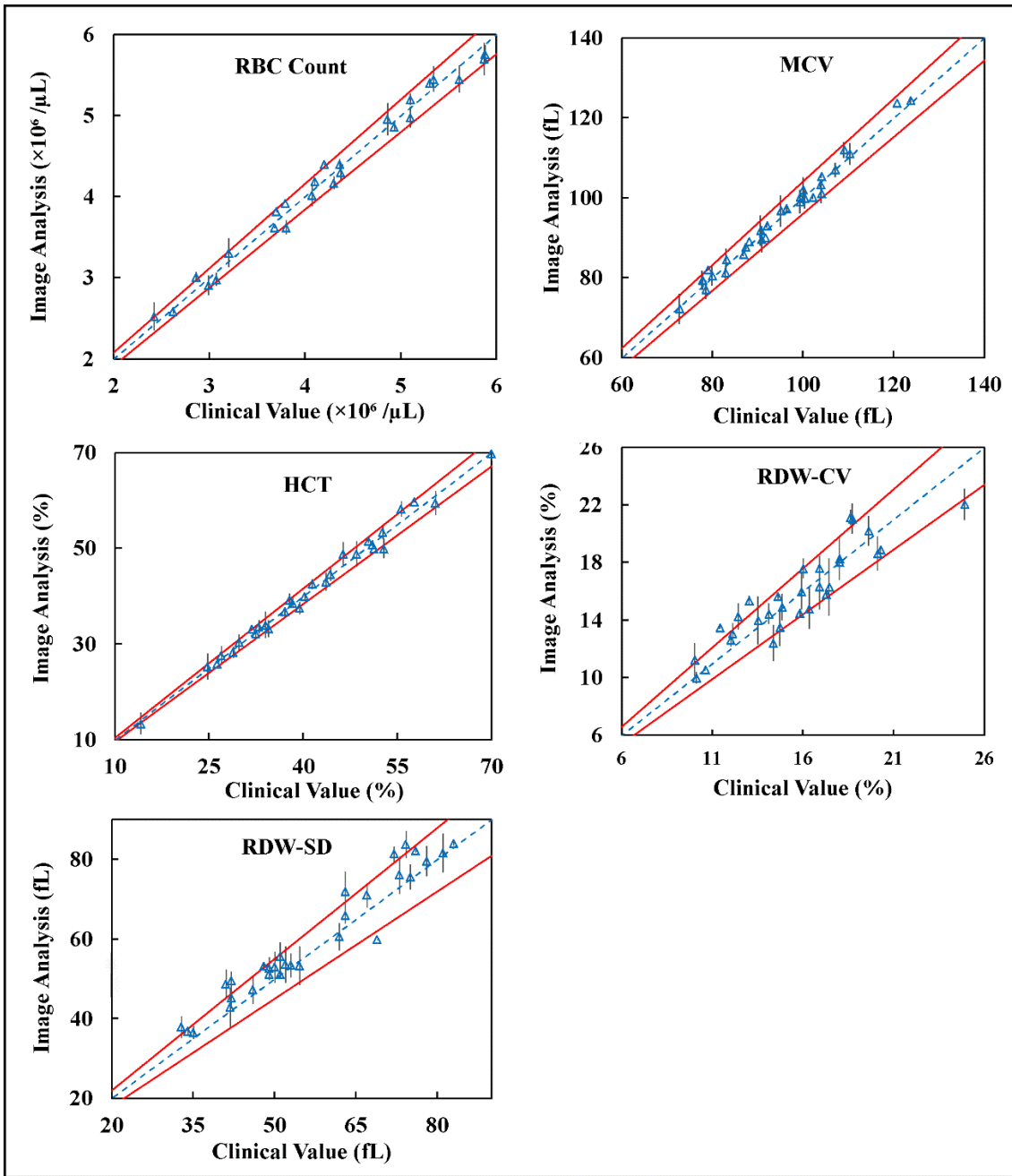


**Figure S6.** RBC count MCV, HCT, RDW-CV, and RDW-SD result comparison with clinical results.

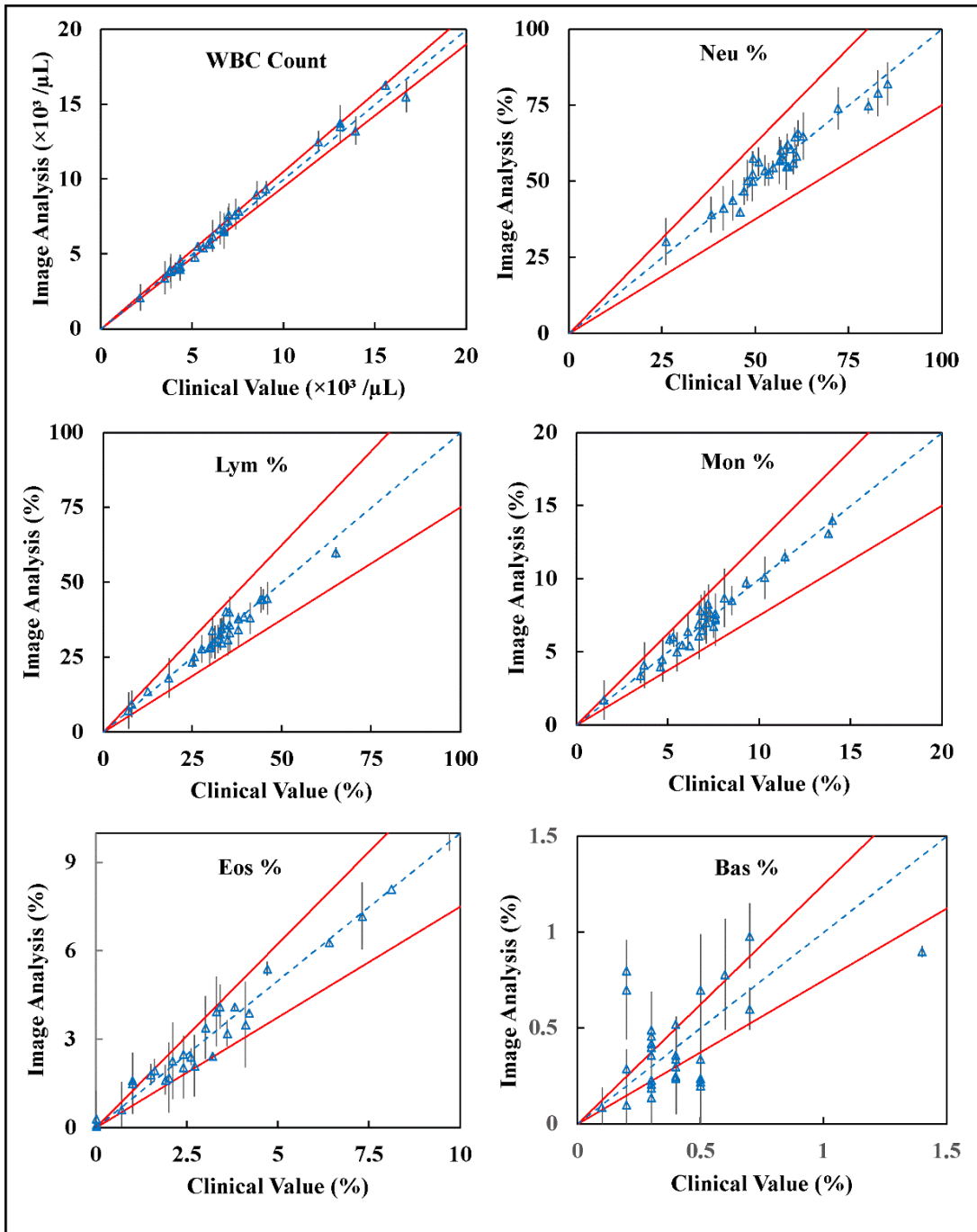


Figure S7. WBC's including subpopulations result comparison with clinical results.